Research Article Vol. 33, No. 1 / /Journal of the Optical Society of America B 1

Journal of the Optical Society of America B

OPTICAL PHYSICS

Spontaneous parametric downconversion and quantum walk topology

GRACIANA PUENTES

Departamento de Fisica, Facultad de Ciencias Exactas y Naturales, Pabellón 1, Ciudad Universitaria, 1428 Buenos Aires, Argentina (gracianapuentes@gmail.com)

Received 27 October 2015; revised 12 January 2016; accepted 12 January 2016 (Doc. ID 252728); published 0 MONTH 0000

We propose a novel scheme for the *all-optical* quantum simulation of topological phases by means of implementation of a discrete-time quantum walk architecture. The main novel ingredient is the inclusion of the nonlinear process of spontaneous parametric downconversion (SPDC) along the quantum network. By means of a simple theoretical model, the interplay between quantum walk lattice topology and spatial correlations of biphotons produced by SPDC is numerically explored. We describe different *optical* detection methods suitable for the implementation of our proposed experimental scheme.

OCIS codes: (270.0270) Quantum optics; (270.6620) Strong-field processes; (270.4180) Multiphoton processes.

http://dx.doi.org/10.1364/JOSAB.99.099999

1. INTRODUCTION

Spontaneous parametric downconversion (SPDC) is a standard technique in quantum optics. It results from the absorption and spontaneous conversion of a pump incident photon in a nonlinear crystal or fiber, producing in this manner two lower energy photons (the so-called signal and idler). The pairs of downconverted photons can be entangled in a multiparameter space of frequency, momentum, and polarization [1–3,4]. In Type II SPDC, the signal and idler photons are entangled in frequency, and wave and momentum have orthogonal polarizations. In noncollinear Type II SPDC, the signal and idler photons are entangled as well in polarization. Entangled photons have been used to demonstrate quantum nonlocality [5,6], quantum teleportation [7–9], quantum information processing [10–12], and quantum cryptography [13,14]. Recently there has been much interest in controlling temporal and spatial properties of entangled photons either by spectral filtering with narrowband filters [15,16], tailored dispersion in photonic crystal fibers [17], or by placing the nonlinear media in cavities [18]. Temporal shaping has also been achieved using spectral phase modulation of signal or idler photons produced in Type I collinear parametric downconversion [19].

Random walks have been used to model a variety of dynamic physical processes containing some form of stochasticity, including phenomena such as Brownian motion and the transition from binomial to Gaussian distribution in the limit of large statistics. The quantum walk (QW) is the quantum analogue of the random walk, where the classical walker is replaced by a quantum particle, such as a photon or an electron, and the stochastic evolution is replaced by a unitary process. The stochastic ingredient is added by introducing some internal degrees of freedom that can be stochastically flipped during the evolution, which is usually referred to as a quantum coin. One of the main features of QWs is that the different paths of the quantum walker can interfere and therefore present a complicated (non-Gaussian) probability distribution for the final position of the walker after a number of discrete steps. In recent years, QWs have been successfully implemented to simulate a number of quantum phenomena, such as photosynthesis [20], quantum diffusion [21], vortex transport [22], and electrical breakdown [23], and they have provided a robust platform for the simulation of quantum algorithms and maps [24]. QWs have been experimentally implemented in the context of nuclear magnetic resonance (NMR) [25], cavity quantum electrodynamics (QED) [26], trapped ions [27,28], cold atoms [29], and optics, both in the spatial [30] and frequency domains [12]. In recent years, QWs with single and correlated photons have been successfully introduced using waveguides [31] and bulk optics [32], and time-domain implementations [33]. Moreover, discrete-time quantum walks (DTQWs) [34] offer a versatile platform for the exploration of a wide range of nontrivial geometric and topological phenomena (experiment [27,35,36] and theory [37–41]). Further, QWs are robust platforms for modeling a variety of dynamic processes from excitation transfer in spin chains [42,43] to energy transport in biological complexes [44]. They enable study of multipath quantum interference phenomena [45–48], and can provide for a route to validation of quantum complexity [49,50] and universal quantum computing [51]. Moreover, multiparticle QWs warrant a powerful tool for encoding information in an exponentially larger space, and for quantum simulations in biological, chemical, and physical systems, in 1D and 2D geometries [31,52].

In this paper, we propose a detailed research program for the study for nonlinear effects in photonic QWs and their interplay with topological phenomena [53–55]. More specifically, we analyze the interplay between a nontrivial topology, determined by the unitary step of a linear QW Hamiltonian (H_{QW}), and the phase-matching condition characterizing biphotons produced by the nonlinear process of spontaneous parametric down conversion (SPDC) characterized by a nonlinear Hamiltonian (H_{SPDC}). By considering both linear and nonlinear contributions in the overall biphoton Hamiltonian, we analyze the coupling efficiency and emission probability in different topological scenarios, determined by the linear Hamiltonian. It is relevant to point out that most implementations of a QW [12,21–24,26,29,31–33,56,52] have introduced passive linear elements *only* for the composing elements of the random network, with the exception of a few remarkable recent contributions [57].

The unitary step in the DTQW characterizing the linear Hamiltonian (H_{QW}) consists of a sequence of rotations and spin-dependent translations. This is implemented by means of two half-wave plates and two (calcite or fiber) polarization beam splitters, respectively, as proposed by Kitagawa *et al.* [37]. This simple unitary step has readily been shown to display nontrivial topology [35,37]. It is beyond the scope of this article to repeat the derivation that demonstrates the nontrivial topology of the basic unitary step. We refer the interested reader to Refs. [35,37] for further information on the topology of the linear Hamiltonian. This unitary step is then repeated a number of times along the DTQW, by concatenating the same sequence of beam splitters and wave plates. The number of times (T) this unitary step is repeated represents the number of discrete steps in the DTQW (see Fig. 1 for reference). Once the unitary step is given, we find the eigenvectors of the linear Hamiltonian (H_{QW}) (Bloch vectors); this will determine, in turn, the basis for decomposing the nonlinear Hamiltonian, as well the phase-matching condition for maximizing the coupling efficiency. We note that for the particular topology we analyze here $n_z = 0$, the Bloch vectors are phasors, which depend only on a relative phase $\phi(k)$. The array of spatial modes (n) defined by the sequence of beam splitters in the DTQW determines, in turn, the underlying lattice network for our analysis. We note that there is no evanescent coupling between the different spatial modes. In addition to the linear term in the DTQW Hamiltonian, which fully determines the topology of the system and was analyzed in detail in Refs. [35,37], we analyze the contribution of a nonlinear spontaneous parametric downconversion (SPDC) term. This is in contrast to the seminal work by Kitagawa *et al.* [37], which considers propagation of only a single photon, and does not analyze SPDC biphoton contributions. The nonlinear SPDC Hamiltonian (H_{SPDC}) is decomposed as a linear sum of Bloch vectors, which determines a Bloch wave. We then analyze the coupling efficiency Γ of this SPDC Bloch wave to the nth lattice mode. For the particular topology we analyze here ($n_z = 0$), and considering only two spatial modes $n = 1, 2$ in the lattice, the coupling efficiency is fully determined by the phase-matching condition, which is fixed by the relative phase between Bloch vectors $\phi(k)$ and is fully determined by the topology of the unitary step. Therefore, different topologies dictated by the unitary step in H_{QW} determine different phase-matching conditions. We emphasize that the underlying lattice of spatial modes corresponds to the modes dictated by the beam-splitter array. There is no evanescent coupling between the different spatial modes. Moreover, since it is not an array of nonlinear waveguides, there is no upconversion along the lattice of linear spatial modes.

A full class of topological insulators can be realized in a system of noninteracting particles, with a binary (pseudo) spin space for (bosons) fermions, via a random walk of discrete time unitary steps as described in Ref. [37]. The particular type of phase is determined by the size of the system (1D or 2D) and by the underlying symmetries characterizing the Hamiltonian, such as particle-hole symmetry (PHS), time-reversal symmetry (TRS), or chiral symmetry (CS). The 1D DTQW can be specified by a series of unitary spin-dependent translations T and rotations $R(\theta)$, where θ specifies the rotation angle. Thus, the quantum evolution is determined by applying a series of unitary operations or steps:

$$U(\theta) = TR(\theta). \tag{1}$$

The generator of the unitary evolution operator (or map) in Eq. (1) is the time-independent Hamiltonian $H(\theta)$, for which the discrete time evolution operator $U(\theta)$ can be defined as

$$U(\theta) = e^{-iH(\theta)\delta t}, \tag{2}$$

where we have chosen $\hbar = 1$, and the finite time evolution after N steps is given by $U^N = e^{-iH(\theta)N\delta t}$.

The Hamiltonian $H(\theta)$ determined by the translation and rotation steps T and $R(\theta)$, possess PHS for some operator P (i.e., $PHP^{-1} = -H$) and it also contains CS. The presence of PHS and CS guarantees TRS. The presence of TRS and PHS imply that the system belongs to a topological class contained in the Su–Schrieffer–Heeger (SSH) model [58] and can thus be employed to simulate a class of SSH topological phase. An extension to 2D topological insulators can be obtained by extending the lattice of sites to 2D. Different geometries, such as square lattice or triangular lattice, are described in Ref. [37]. In this work we propose to study the dynamical evolution given a general overall Hamiltonian of the form

$$H = H_{\mathrm{QW}} + H_{\mathrm{SPDC}}, \tag{3}$$

where the first term is the linear contribution given by the nontrivial topology of the QW lattice, and the second term is the nonlinear contribution due to the SPDC in nonlinear media along the lattice.

2. SPLIT-STEP QW HAMILTONIAN (H_{QW})

The topology of the DTQW is fully determined by the unitary step in the DTQW. The unitary step is indicated in Fig. 1 by a dashed box. This unitary step consists of a rotation, typically implemented by means of a half-wave plate (HWP), and a polarization-dependent translation, typically implemented by a calcite beam splitter [Fig. 1(a)] or by a fiber beam splitter [Fig. 1(a)]. We stress that there is no evanescent coupling between the linear network of spatial modes defined by the array of beam splitters.

The basic step in the standard DTQW is given by a unitary evolution operator $U(\theta) = TR_{\vec{n}}(\theta)$ [35,37], where $R_{\vec{n}}(\theta)$ is a rotation along an arbitrary direction $\vec{n} = (n_x, n_y, n_z)$, given by

$$R_{\vec{n}}(\theta) = \begin{pmatrix} \cos(\theta) - in_z \sin(\theta) & (in_x - n_y)\sin(\theta) \\ (in_x + n_y)\sin(\theta) & \cos(\theta) + in_z \sin(\theta) \end{pmatrix}, \quad (4)$$

in the Pauli basis [59]. In this basis, the y rotation is defined by a coin operator of the form

$$R_y(\theta) = \begin{pmatrix} \cos(\theta) & -\sin(\theta) \\ \sin(\theta) & \cos(\theta) \end{pmatrix}. \quad (5)$$

This is followed by a spin- or polarization-dependent translation T given by

$$T = \sum_x |x+1\rangle\langle x| \otimes |H\rangle\langle H| + |x-1\rangle\langle x| \otimes |V\rangle\langle V|, \quad (6)$$

where $H = (1, 0)^T$ and $V = (0, 1)^T$. The evolution operator for a discrete-time step is equivalent to that generated by a Hamiltonian $H(\theta)$, such that $U(\theta) = e^{-iH(\theta)}$ ($\hbar = 1$), with

$$H_{\mathrm{QW}}(\theta) = \int_{-\pi}^{\pi} \mathrm{d}k [E_\theta(k)\vec{n}(k).\vec{\sigma}] \otimes |k\rangle\langle k|, \quad (7)$$

and $\vec{\sigma}$ the Pauli matrices, which readily reveals the spin–orbit coupling mechanism in the system. The QW described by $U(\theta)$ has been realized experimentally in a number of systems [27,29,32,33], and has been shown to possess CS and display a Dirac-like dispersion relation given by $\cos(E_\theta(k)) = \cos(k)\cos(\theta)$.

Here we analyze a DTQW protocol consisting of two consecutive spin-dependent translations T and rotations R, such that the unitary step becomes $U(\theta_1, \theta_2) = TR(\theta_1)TR(\theta_2)$. The so-called "split-step" QW, has been shown to possess a nontrivial topological landscape characterized by topological sectors with different topological numbers, such as the winding number $W = (0, 1)$ [37]. The dispersion relation for the split-step QW results in [37]

$$\cos(E_{\theta,\phi}(k)) = \cos(k)\cos(\theta_1)\cos(\theta_2) - \sin(\theta_1)\sin(\theta_2). \quad (8)$$

The 3D norm for decomposing the QW Hamiltonian of the system in terms of Pauli matrices $H_{\mathrm{QW}} = E(k)\vec{n}\cdot\vec{\sigma}$ becomes [37]

$$\begin{aligned} n^x_{\theta_1,\theta_2}(k) &= \frac{\sin(k)\sin(\theta_1)\cos(\theta_2)}{\sin(E_{\theta_1,\theta_2}(k))}, \\ n^y_{\theta_1,\theta_2}(k) &= \frac{\cos(k)\sin(\theta_1)\cos(\theta_2) + \sin(\theta_2)\cos(\theta_1)}{\sin(E_{\theta_1,\theta_2}(k))}, \\ n^z_{\theta_1,\theta_2}(k) &= \frac{-\sin(k)\cos(\theta_2)\cos(\theta_1)}{\sin(E_{\theta_1,\theta_2}(k))}. \end{aligned} \quad (9)$$

Diagonalization of H_{QW} gives the lattice Bloch eigenvectors that characterize the QW Hamiltonian, resulting in

$$\mathbf{u}_\pm(k) = \frac{1}{\mathcal{N}}\left(1, \frac{n_x(k) + in_y(k)}{n_z(k) \pm \lambda(k)}\right)^T, \quad (10)$$

with $\lambda^2 = n_x^2 + n_y^2 + n_z^2$, and $\mathcal{N}$ as a normalization factor. We note that the relation between the two components of $\mathbf{u}_\pm$ will eventually determine the phase-matching condition for down-converted photons, and for this reason it is of relevance for our analysis.

For the particular case that $n_z(k) = 0$, the eigenvectors take the simple form

$$\mathbf{u}_\pm(k) = \frac{1}{\sqrt{2}}(1, e^{-i\phi(k)})^T, \quad (11)$$

with $\phi(k) = \mathrm{atan}(\frac{n_y}{n_x})$. For the split-step QW, this relative phase results in

$$\tan(\phi(k)) = \frac{\cos(k)\sin(\theta_1)\cos(\theta_2) + \sin(\theta_2)\cos(\theta_1)}{\sin(k)\sin(\theta_1)\cos(\theta_2)}. \quad (12)$$

3. SPDC HAMILTONIAN (H_{SPDC})

We can decompose the nonlinear Hamiltonian H_{SPDC} in terms of the Bloch eigenvectors $\mathbf{u}_\pm(k)$ by defining Bloch waves of the form $\hat{A}_p(k) = \sum_n \hat{\mathbf{a}}_\mathbf{n}\mathbf{u}_\pm(k)e^{ikn}$, with $\hat{\mathbf{a}}_\mathbf{n} = (\hat{a}_{n,1}, \hat{a}_{n,2}, \ldots, \hat{a}_{N,m})$ and $\hat{a}_{N,m}$ the annihilation operator of the mth sublattice mode.

We stress that the different sublattice modes correspond to the linear network of spatial modes defined by the array of beam splitters used at each unitary step (see Fig. 1). The network does not correspond to an array of nonlinear waveguides, and, therefore, there is no evanescent coupling or upconversion between the different spatial modes. In Fig. 1 we consider a single SPDC event; however, additional SPDC events could be considered in the case of fiber beam splitters filled with nonlinear active media, as described in Section 5.A.

The SPDC Hamiltonian results in

$$H_{\mathrm{SPDC}} = \sum_{p_{s,i}} \int \mathrm{d}k_s \int \mathrm{d}k_i \Gamma_{p_{s,i}}(k_s, k_i)\hat{A}^\dagger_{p_s}(k_s)\hat{A}^\dagger_{p_i}(k_i), \quad (13)$$

where the coupling efficiency $\Gamma_{p_{s,i}}(k_s, k_i)$ to the Bloch wave results in the contribution of N sublattices of the form

$$\Gamma_{p_{s,i}}(k_s, k_i) = \gamma \sum_{n=1}^{N} E^p_n(k_s + k_i)u_{p_s,j}(k_s)u_{p_i,j}(k_i). \quad (14)$$

For the case of a pump mode coupled to only two sublattices labeled by $n = 1, 2$, substituting the eigenmode profile determined by the topology of the QW Hamiltonian $u_{s,i}$, we obtain an expression for $\Gamma_{p_{s,i}}(k_s, k_i)$ of the form

$$\Gamma_{p_{s,i}}(k_s, k_i) = \gamma\left(E^p_1(k_s + k_i) + E^p_2(k_s + k_i)\frac{n_x(k) + in_y(k)}{n_z(k) \pm \lambda(k)}\right). \quad (15)$$

For the particular case that $n_z = 0$, we obtain the simplified expression

$$\Gamma_{p_{s,i}}(k_s, k_i) = \gamma(E^p_1(k_s + k_i)e^{-i|\phi_s(k)+\phi_i(k)|} + E^p_2(k_s + k_i)), \quad (16)$$

where $\phi_{s,i}(k)$ are the phase-matching functions for signal and idler, which depend on the QW topology. For the particular case of the split-step QW, this results in Eq. (12) for each of the biphotons independently.

4. NUMERICAL RESULTS

In Ref. [37] the authors demonstrate that the unitary step in the DTQW we consider has a nontrivial topology. The nontrivial topology of the unitary step is typically demonstrated by calculating pertinent topological invariants. For the case of 1D systems, the topological invariant is the winding number W. Kitagawa *et al.* [37] showed that the winding number in the unitary step we consider here takes two different values, $W = 0$ or $W = 1$ [38]. The value of the winding number W defines topological sectors, since a topological sector can be defined as a region in parameter space where the topological invariant takes a fixed value. The existence of two different discrete values for this topological invariant W demonstrates a nontrivial topological landscape. We refer the interested reader to the seminal work by Kitagawa *et al.* [37] for further details on the topological aspects of the unitary step considered here. In this section we analyze the impact of the unitary step topology, by considering DTQW parameters $\theta_{1,2}^{s,i}$ belonging to the same topological sector, $W = 0$ or $W = 1$, as well as to different topological sectors corresponding to different values of the winding number $W = 0, 1$.

We first performed simulations to quantify the impact of the pump envelope $E_1^p(k_s + k_i)$ on the coupling efficiency $\Gamma_{p_{s,i}}(k_s, k_i)$. This, in turn, can provide information about the spatial correlations between the biphotons produced by SPDC, since the efficiency is proportional to the probability amplitude of emission of biphotons. In all simulations we assumed a sufficiently large crystal length L, so that the sinc dependence of the phase-matching function is maximal and can be considered constant. This is illustrated in Fig. 2, for $(\theta_1^{s,i} = 0.01, \theta_2^{s,i} = 0.0001)$, for two different pump envelope widths $\sigma = 500$ and $\sigma = 10$, and for different relative phases between the signal and idler $\phi_s(k) = \pm\phi_i(k)$. In Fig. 2(a), $\theta_1^{s,i} = 0.01$, $\theta_2^{s,i} = 0.001$, $\phi_s(k) = \phi_i(k)$, and pump envelope width $\sigma = 500$; in Fig. 2(b), $\theta_1^{s,i} = 0.01$, $\theta_2^{s,i} = 0.001$, $\phi_s(k) = -\phi_i(k)$, and pump envelope width $\sigma = 500$; in Fig. 2(c), $\theta_1^{s,i} = 0.01$, $\theta_2^{s,i} = 0.001$, $\phi_s(k) = \phi_i(k)$, and pump envelope width $\sigma = 10$; and in Fig. 2(d), $\theta_1^{s,i} = 0.01$, $\theta_2^{s,i} = 0.001$, $\phi_s(k) = -\phi_i(k)$, and pump envelope width $\sigma = 10$. It is apparent that a small envelope reduces coupling efficiency to only the large values of momentum for signal and idler. On the other hand, as expected, as the width σ of the pump envelope increases, so does the coupling efficiency.

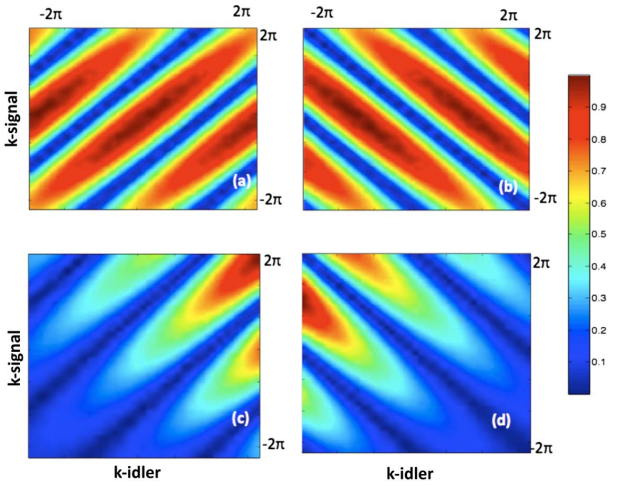

Fig. 2. Numerical simulation of coupling efficiency $\Gamma_{p_{s,i}}(k_s, k_i)$ in Fourier domain. (a) $\theta_1^{s,i} = 0.01$, $\theta_2^{s,i} = 0.001$, $\phi_s(k) = \phi_i(k)$ and pump envelope width $\sigma = 500$, (b) $\theta_1^{s,i} = 0.01$, $\theta_2^{s,i} = 0.001$, $\phi_s(k) = -\phi_i(k)$ and pump envelope width $\sigma = 500$, (c) $\theta_1^{s,i} = 0.01$, $\theta_2^{s,i} = 0.001$, $\phi_s(k) = \phi_i(k)$ and pump envelope width $\sigma = 10$, (d) $\theta_1^{s,i} = 0.01$, $\theta_2^{s,i} = 0.001$, $\phi_s(k) = -\phi_i(k)$ and pump envelope width $\sigma = 10$.

In order to further analyze the impact of the QW lattice topology on the type of coupling efficiency that can be expected, we performed simulations considering a constant amplitude for the pump, $E^p(k_s + k_i) = E^p$, with no dependence on k in Fourier space. We consider two cases, corresponding to phase parameters $\theta_{1,2}^{s,i}$ defining different phase-matching conditions $\phi_{s,i}(k)$ for signal and idler photons. This is illustrated in Fig. 3: in Fig. 3(a), $\theta_1^{s,i} = 0.01$, $\theta_2^{s,i} = 9 \times \pi/20$, and $\phi_s(k) = \phi_i(k)$; in Fig. 3(b), $\theta_1^{s,i} = 0.01$, $\theta_2^{s,i} = 0.001$, and $\phi_s(k) = \phi_i(k)$; in Fig. 3(c), $\theta_1^{s,i} = 0.01$, $\theta_2^{s,i} = 9 \times \pi/20$, and $\phi_s(k) = -\phi_i(k)$; and in Fig. 3(d), $\theta_1^{s,i} = 0.01$, $\theta_2^{s,i} = 0.001$, and $\phi_s(k) = -\phi_i(k)$. Figure 3 reveals the emergence of a nontrivial 2D grid in the coupling efficiency for QW lattice parameters in distinct topological sectors [Figs. 3(a) and 3(c)]. The periodicity in the grid is a clear consequence of the periodicity in lattice parameters and k space. On the other hand, for lattice parameters in the same topological sector [Figs. 3(b) and 3(d)], we obtain the same type of coupling coefficient as expected for standard SPDC, with, of course, no k-dependence since this was ignored in the approximation of constant pump envelope $E^p(k_s + k_i) = E^p$.

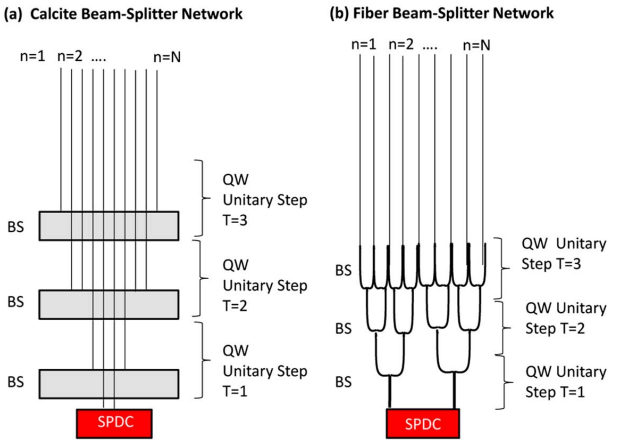

Fig. 1. Experimental scheme for implementation of DTQW based on (a) a sequence of calcite beam splitters, and (b) a sequence of fiber beam splitters. While the lattice itself is defined by the spatial modes characterizing the array of beam splitters, the lattice topology is fully determined by the unitary step in the QW, indicated with a dashed box. We note that there is no evanescent coupling or upconversion between the different spatial modes determined by the beam-splitter network. This experimental scheme can be employed for measurement of spatial correlation via coincidence counts between different sublattice modes (n).

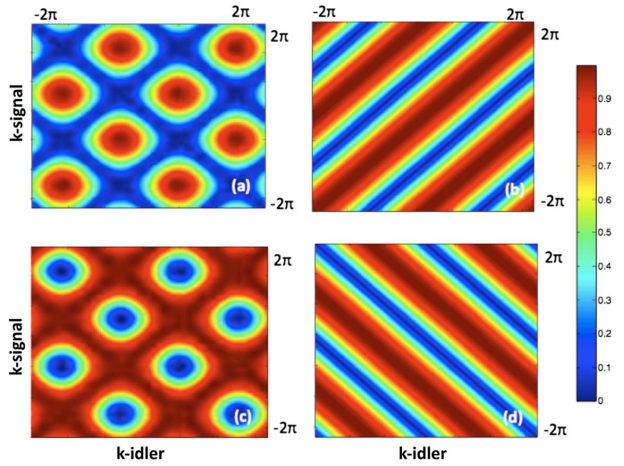

Fig. 3. Numerical simulation of coupling efficiency $\Gamma_{p_s,i}(k_s, k_i)$ in the Fourier domain. (a) $\theta_1^{s,i} = 0.01$, $\theta_2^{s,i} = 9 \times \pi/20$, and $\phi_s(k) = \phi_i(k)$. (b) $\theta_1^{s,i} = 0.01$, $\theta_2^{s,i} = 0.001$, and $\phi_s(k) = \phi_i(k)$. (c) $\theta_1^{s,i} = 0.01$, $\theta_2^{s,i} = 9 \times \pi/20$, and $\phi_s(k) = -\phi_i(k)$, $\theta_1^{s,i} = 0.01$. (d) $\theta_1^{s,i} = 0.01$, $\theta_2^{s,i} = 0.001$, and $\phi_s(k) = -\phi_i(k)$.

5. EXPERIMENTAL METHODS

A. Fiber Network

In Ref. [32] the authors performed an optical implementation of the operator defined by Eq. (1), using polarization degrees of freedom of single photons and a sequence of half-wave plates and calcite beam splitters. On the other hand, in Ref. [31], the authors implemented a QW in a lattice of coupled wave guides. In this work, we propose to use a fiber network to implement a QW to simulate 1D and 2D topological phases. One of the main ingredients is the implementation of an optical nonlinearity that can introduce the production of biphotons, for instance, via the process of SPDC as described in the previous sections. The nonlinear contribution can be considered a single SPDC event (see Fig. 1), or it can be introduced sequentially along the network by using, for instance, fiber beam splitters filled with active media. We note that there is no evanescent coupling between the spatial modes defined by the beam splitters, and therefore no evanescent coupling between two hollow-core fibers is required. We argue that, in this way, one could simulate both attractive and repulsive interactions (for the cases of correlated or anticorrelated down-converted biphotons). A similar idea was already proposed in Ref. [60], where attractive interactions were introduced in a planar AlGaAs waveguide characterized by a strong focusing Kerr nonlinearity. Likewise, repulsive interactions can be simulated using defocusing nonlinearities [60], though this would remain part of future efforts. A suitable alternative waveguide for the simulation of attractive interactions is a photonic bandgap fiber with a Raman active gas, which is predicted to have a strong nonlinearity. These fibers consist of hollow-core photonic crystal fibers filled with an active Raman gas, which are capable of exceeding intrinsic Kerr nonlinearities by orders of magnitude [61,62].

B. Input State Preparation

For the linear (noninteracting) case [QW with SU(2) symmetry] we plan to use single-mode states both with Poissonian and sub-Poissonian statistics, such as coherent states and squeezed coherent or single-photon states. The nonclassical nature of the squeezed and single-photon states should be revealed in the intensity distribution of counts, as well as in the standard deviation. On the other hand, for the nonlinear (interacting) case [SPDC with SU(1,1) symmetry], quantum theory predicts that the probability amplitudes of the modes should interfere, leading to an enhancement/reduction of the initial correlations. One of the goals of the project is to analyze the sensitivity of the nonlinear network to phase relations dictated by the topology of the network in the input state and to the amount of gain. We also plan to analyze the effect of correlations and entanglement in the input state on localized edge states and to find some kind of nonlocal order parameter characterizing topological order [63]. Finally, one of the aims of this research plan is to demonstrate the feasibility of entanglement topological protection [53].

C. Detection Schemes

1. Intensity Probability Distributions and Standard Deviation

The most direct form of measurement is to detect the statistics of counts by studying intensity histograms of photons and their standard deviation, as described in Refs. [32,60]. In particular, by placing a avalanche photodiode (APD) at the output of each fiber, characterizing a given site in the network, it is possible to obtain a probability distribution of counts and its standard deviation along the N steps of the QW. While in the case of input states with Poissonian statistics we expect to find a classical *binary* distribution of counts as the output of the QW, in the nonclassical case we expect to find a localized edge state at the boundary between two different topological sectors. Furthermore, we plan to measure the normalized standard deviation σ_N for the classical and nonclassical case, where we expect to find a markedly different dependence on the number of steps N; namely, while for the classical walk (coherent states) we plan to obtain $\sigma_N \propto \sqrt{N}$ diffusive dependence, for the nonclassical case (squeezed states, single photons) we plan to obtain an $\sigma_N \propto N$ ballistic dependence with the number of discrete steps.

2. HBT Correlation Measurements

When using nonlinear fibers in the amplifying network, it would be interesting to analyze one-mode ($g^1(\Delta r)$) and two-mode ($g^2(\Delta r)$) spatial correlations functions by means of Hanbury Brown–Twiss (HBT)-like interferometers between different output modes in the network, as described in Ref. [60]. In particular, while in the case of attractive interactions, as simulated by Kerr nonlinearities in fibers, the correlations are expected to increase, for the repulsive case the correlations are expected to decrease. We also plan to analyze the dependence of spatial correlations on the amount of gain present in the medium. In particular, for some critical value of the overall gain G_c, we expect to find a decay of the correlations, which in turn can be related to the classical–quantum transition in amplifying media [62]. Finally, we will also investigate the response of the amplifying network to different phases in the input states dictated in turn by the topology

of the network, as well as the response to phase noise, by introducing phase-averaging mechanisms.

6. DISCUSSION AND OUTLOOK

In this work we propose an experimental implementation of topological phases by means of an optical implementation of a discrete-time quantum walk (DTQW) architecture. One of the main novel ingredients is the inclusion of nonlinear media and nonlinear effects in the DTQW via the possibility of spontaneous parametric downconversion (SPDC) in the lattice. By means of numerical simulations, we have analyzed the interplay between quantum walk (QW) topology and spatial properties of photon pairs produced by SPDC. In particular, we have numerically described how the topology of the QW lattice can play an important role in the phase-matching function of biphotons produced by SPDC. As a future work, we expect to characterize the robustness of such topological phases and their characteristic bound states against amplitude and phase noise, as well as to decoherence, by tracing over spatial modes of the field. One of the main goals of the proposed work is to investigate the use of parametric amplifiers as a means of simulating many-body effects in topological phases. In particular, we expect to link such phases with the classical or quantum statistics of the fields by means of intensity distribution and spatial correlation measurements, and we intend to find a link between some measure of entanglement and a nonlocal order parameter characterizing the topology of the phase [63], or the feasibility of entanglement topological protection approaches [53]. Some significant signatures of many-body dynamics in topological order are expected to be apparent, such as charge fractionalization and Hall quantization, which motivate the extension of the research to the nonlinear (many-body) scenario. Furthermore, other more complex topological phases (such as spin-Hall phase) could be simulated in the future by all-optical means by using 2D QWs and higher dimensional internal degrees of freedom of the radiation field, such as the orbital angular momentum [64]. Furthermore, topological order has been considered as a useful ingredient for fault-tolerant quantum computation, as it can protect the system against local perturbations that would otherwise introduce decoherence and loss of quantum information [65].

Funding. Young Investigator (PICT2014-1543); PDE (UBACyT 2015); Raices Programme.

REFERENCES

1. D. C. Burnham and D. L. Weinberg, "Observation of simultaneity in parametric production of optical photon pairs," Phys. Rev. Lett. **25**, 84–87 (1970).
2. Z. Y. Ou, X. Y. Zou, L. J. Wang, and L. Mandel, "Experiment on nonclassical fourth-order interference," Phys. Rev. A **42**, 2957–2965 (1990).
3. C. K. Hong and L. Mandel, "Theory of parametric frequency down-conversion of light," Phys. Rev. A **31**, 2409–2418 (1985).
4. M. H. Rubin, D. N. Klyshko, Y. H. Shih, and A. V. Sergienko, "Theory of two-photon entanglement in type-II optical parametric downconversion," Phys. Rev. A **50**, 5122–5133 (1994).
5. Z. Y. Ou and L. Mandel, "Violation of Bell's inequality and classical probability in a two-photon correlation experiment," Phys. Rev. Lett. **61**, 50–53 (1988).
6. P. G. Kwiat, K. Mattle, H. Weinfurter, A. Zeilinger, A. V. Sergienko, and Y. H. Shih, "New high-intensity source of polarization-entangled photons," Phys. Rev. Lett. **75**, 4337–4341 (1995).
7. C. H. Bennett, G. Brassard, C. Crepeau, R. Jozsa, A. Peres, and W. K. Wootters, "Teleporting an unknown quantum state via classical and Einstein-Podolsky-Rosen channels," Phys. Rev. Lett. **70**, 1895–1899 (1993).
8. L. Braunstein and H. J. Kimble, "Teleportation of continuous quantum variables," Phys. Rev. Lett. **80**, 869–872 (1998).
9. L. Vaidman, "Teleportation of quantum states," Phys. Rev. A **49**, 1473–1476 (1994).
10. D. Bouwmeester, J.-W. Pan, K. Mattle, M. Eibl, H. Weinfurter, and A. Zeilinger, "Experimental quantum teleportation," Nature **390**, 575–579 (1997).
11. J.-W. Pan, D. Bouwmeester, H. Weinfurter, and A. Zeilinger, "Experimental entanglement swapping: entangling photons that never interacted," Phys. Rev. Lett. **80**, 3891–3894 (1998).
12. D. Bouwmeester, J.-W. Pan, M. Daniell, H. Weinfurter, and A. Zeilinger, "Observation of three-photon Greenberger-Horne-Zeilinger entanglement," Phys. Rev. Lett. **82**, 1345–1349 (1999).
13. A. K. Ekert, J. G. Rarity, P. R. Tapster, and G. M. Palma, "Practical quantum cryptography based on two-photon interferometry," Phys. Rev. Lett. **69**, 1293–1295 (1992).
14. W. Tittel, J. Brendel, H. Zbinden, and N. Gisin, "Quantum cryptography using entangled photons in energy-time Bell states," Phys. Rev. Lett. **84**, 4737–4740, 2000.
15. M. Bellini, F. Marin, S. Viciani, A. Zavatta, and F. T. Arecchi, "Nonlocal pulse shaping with entangled photon pairs," Phys. Rev. Lett. **90**, 043602 (2003).
16. A. Peter, B. Dayan, A. Friesem, and Y. Silberberg, "Temporal shaping of entangled photons," Phys. Rev. Lett. **94**, 073601 (2005).
17. O. Cohen, J. Lundeen, B. Smith, G. Puentes, P. Mosley, and I. Walmsley, "Tailored photon-pair generation in optical fibers," Phys. Rev. Lett. **102**, 123603 (2009).
18. R. Andrews, E. R. Pike, and S. Sarkar, "Photon correlations of a subthreshold optical parametric oscillator," Opt. Express **10**, 461–468 (2002).
19. A. V. Sergienko, Y. H. Shih, and M. H. Rubin, "Experimental evaluation of a two-photon wave packet in type-II parametric down-conversion," J. Opt. Soc. Am. B **12**, 859–862 (1995).
20. M. Mohseni, P. Rebentrost, S. Lloyd, and A. Aspure-Guzik, "Environment-assisted quantum walks in photosynthetic energy transfer," J. Chem. Phys. **129**, 174106 (2008).
21. S. Godoy and S. Fujita, "Quantum random walk and transient phenomena," Phys. A **196**, 416–426 (1993).
22. M. Rudner and L. S. Levitov, "Topological transition in a non-Hermitian quantum walk," Phys. Rev. Lett. **102**, 065703 (2009).
23. T. Oka and N. Nagaosa, "Interfaces of correlated electron systems: proposed mechanism for colossal electroresistance," Phys. Rev. Lett. **95**, 137601 (2005).
24. L. Ermann, J. P. Paz, and M. Saraceno, "Decoherence induced by a chaotic environment: a quantum walk with complex coin," Phys. Rev. A **73**, 012302 (2006).
25. C. Ryan, M. Laforest, J. C. Boileau, and R. Laflamme, "Experimental implementation of discrete-time quantum random walk on an NMR quantum information processor," Phys. Rev. A **72**, 062317 (2005).
26. G. Agarwal and P. Pathak, "Quantum random walk of the field in an external driven cavity," Phys. Rev. A **72**, 033815 (2005).
27. H. Schmitz, R. Matjeschk, C. Schneider, J. Glueckert, M. Enderlein, T. Huber, and T. Schaetz, "Quantum walk of trapped ion in phase space," Phys. Rev. Lett. **103**, 090504 (2009).
28. F. Zaehringer, F. Kirchmair, R. Gerritsma, E. Solano, R. Blatt, and C. Ross, "Realization of quantum with one and two trapped ions," Phys. Rev. Lett. **104**, 100503 (2010).
29. M. Karski, L. Foerster, J.-M. Choi, A. Steffen, W. Alt, and D. Meschede, "Quantum walk in position space with single optically trapped atoms," Science **325**, 174–177 (2009).
30. B. Do, M. L. Stohler, S. Balasubramanian, D. S. Elliott, C. Eash, E. Fischbach, M. A. Fischbach, A. Mills, and B. Zwickl, "Experimental realization of a quantum quincux by use of linear optical elements," J. Opt. Soc. Am. B **22**, 499–504 (2005).

31. A. Peruzzo, M. Lobino, J. C. F. Matthews, N. Matsuda, A. Politi, K. Poulios, X.-Q. Zhou, Y. Lahini, N. Ismail, K. Wöhoff, Y. Bromberg, Y. Silberberg, M. G. Thompson, and J. L. O'Brien, "Quantum walk of correlated particles," Science **329**, 1500–1503 (2010).
32. M. A. Broome, A. Fedrizzi, B. P. Lanyon, I. Kassal, A. Aspuru-Guzik, and A. White, "Discrete single-photon quantum walks with tunable decoherence," Phys. Rev. Lett. **104**, 153602 (2010).
33. A. Schreiber, K. Cassemiro, V. Potocek, A. Garbis, P. J. Mosley, E. Andersson, I. Jex, and C. Silberhorn, "Photons walking the line: a quantum walk with adjustable coin operations," Phys. Rev. Lett. **104**, 050502 (2010).
34. Y. Aharonov, L. Davidovich, and N. Zagury, "Quantum random walks," Phys. Rev. A **48**, 1687–1690 (1993).
35. T. Kitagawa, M. A. Broome, A. Fedrizzi, M. S. Rudner, E. Berg, I. Kassal, A. Aspuru-Guzik, E. Demler, and A. White, "Observation of topologically protected bound states in photonic quantum walks," Nat. Commun. **3**, 882 (2012).
36. M. Genske, W. Alt, A. Steffen, A. H. Werner, R. F. Werner, D. Meschede, and A. Alberti, "Electric quantum walks with individual atoms," Phys. Rev. Lett. **110**, 190601 (2013).
37. T. Kitagawa, M. Rudner, E. Berg, and E. Demler, "Exploring topological phases with quantum walks," Phys. Rev. A **82**, 033429 (2010).
38. H. Obuse and N. Kawakami, "Topological phases and delocalization of quantum walks in random environments," Phys. Rev. B **84**, 195139 (2011).
39. Y. Shikano, K. Chisaki, E. Segawa, and N. Konno, "Emergence of randomness and the arrow of time in quantum walks," Phys. Rev. A **81**, 062129 (2010).
40. J. K. Asbóth, "Symmetries, topological phases and bound states in the one-dimensional quantum walk," Phys. Rev. B **86**, 195414 (2012).
41. A. Wójcik, T. Luckaz, P. Kurzynski, A. Grudka, T. Gdala, and M. Bernarska-Bezdega, "Trapping a particle of a quantum walk on the line," Phys. Rev. A **85**, 012329 (2012).
42. S. Bose, "Quantum communication through an unmodulated spin chain," Phys. Rev. Lett. **91**, 207901 (2003).
43. M. Christandl, N. Datta, A. Ekert, and A. J. Landahl, "Perfect transfer of arbitrary states in quantum spin networks," Phys. Rev. Lett. **92**, 187902 (2004).
44. M. B. Plenio and S. F. Huelga, "Dephasing assisted transport: quantum network and biomolecules," New. J. Phys. **10**, 113019 (2008).
45. J. B. Spring, B. J. Metcalf, P. C. Humphreys, W. S. Kolthammer, X.-M. Jin, M. Barbieri, A. Datta, N. Thomas-Peter, N. K. Langford, D. Kundys, J. C. Gates, B. J. Smith, P. G. R. Smith, and I. A. Walmsley, "Boson sampling on a photonic chip," Science **339**, 798–801 (2013).
46. M. Broome, A. Fedrizzi, S. Rahimi, J. Dove, S. Aaronson, T. Ralph, and A. White, "Boson sampling in a tunable circuit," Science **339**, 794–798 (2013).
47. M. Tillmann, B. Dakic, R. Heilmann, S. Nolte, A. Szameit, and P. Walther, "Experimental boson sampling," Nat. Photonics **7**, 540–544 (2013).
48. A. Crespi, R. Osellame, R. Ramponi, D. J. Brod, E. F. Galvão, N. Spagnolo, C. Vitelli, E. Maiorino, P. Mataloni, and F. Sciarrino, "Integrated multimode interferometers with arbitrary designs for photonic boson sampling," Nat. Photonics **7**, 545–549 (2013).
49. J. Carolan, J. D. A. Meinecke, P. Shadbolt, N. J. Russell, N. Ismail, K. Wörhoff, T. Rudolph, M. G. Thompson, J. L. O'Brien, J. C. F. Matthews, and A. Laing, "On experimental verification of quantum complexity in linear optics," Nat. Photonics **8**, 621–626 (2014).
50. N. Spagnolo, C. Vitelli, M. Bentivegna, D. J. Brod, A. Crespi, F. Flamini, S. Giacomini, G. Milani, R. Ramponi, P. Mataloni, R. Osellame, E. F. Galvao, and F. Sciarrino, "Efficient experimental validation of photonic boson sampling against the uniform distribution," Nat. Photonics **8**, 615–620 (2014).
51. A. M. Childs, "Universal computation by quantum walk," Phys. Rev. Lett. **102**, 180501 (2009).
52. A. Schreiber, A. Gabris, P. Rohde, K. Laiho, M. Stefanak, V. Potocek, C. Hamilton, I. Jex, and C. Silberhorn, "A quantum walk simulation of two-particle dynamics," Science **336**, 55–58 (2012).
53. S. Moulieras, M. Lewenstein, and G. Puentes, "Entanglement engineering and topological protection by discrete-time quantum walks," J. Phys. B **46**, 104005 (2013).
54. G. Puentes, "Unraveling the physics of topological phases by quantum walks of light," arXiv:1409.1273 (2014).
55. G. Puentes and O. Santillan, "Zak phase in discrete-time quantum walks," arXiv:1506.08100v2 (2015).
56. A. Schreiber, K. N. Casemiro, V. Potocek, A. Gabris, I. Jex, and C. Silberhorn, "Decoherence and disorder in quantum walks: from ballistic spread to localization," Phys. Rev. Lett. **106**, 180403 (2011).
57. A. Solntsev, F. Setzpfandt, A. Clark, C. W. Wu, M. Collins, C. Xiong, A. Schreiber, F. Katzschmann, F. Eilenberger, R. Schiek, W. Sohler, A. Mitchell, C. Silberhorn, B. Eggleton, T. Pertsch, A. Sukhorukov, D. Neshev, and Y. Kivshar, "Generation of nonclassical biphoton states through cascaded quantum walks on a nonlinear chip," Phys. Rev. X **4**, 031007 (2014).
58. W. Su, J. Schrieffer, and A. Heeger, "Solitons in polyacetylene," Phys. Rev. Lett. **42**, 1698–1701 (1979).
59. M. Nielsen and I. Chuang, *Quantum Computation and Quantum Information* (Cambridge University, 2000).
60. Y. Broomberg, Y. Lahini, E. Small, and Y. Silberberg, "Hanbury-Brown and Twiss inteferometry with interacting photons," Nat. Photonics **4**, 721–726 (2010).
61. D. V. Skryabin, F. Bialanca, D. Bird, and F. Benabid, "Effective Kerr nonlinearity and two-color solitons in photonic band-gap fibers filled with a Raman active gas," Phys. Rev. Lett. **93**, 143907 (2004).
62. A. Regensburger, C. Bersch, M.-A. Miri, G. Onischukov, D. N. Christodoulides, and U. Peschel, "Parity-time synthetic photonic lattices," Nature **488**, 167–171 (2013).
63. H. Li and F. Haldane, "Entanglement spectrum as a generalization of entanglement entropy: Identification of topological order in non-abelian fractional quantum Hall effect states," Phys. Rev. Lett. **101**, 010504 (2008).
64. G. Puentes, N. Hermosa, and J. P. Torres, "Weak measurements with orbital-angular-momentum pointer states," Phys. Rev. Lett. **109**, 040401 (2012).
65. J. Preskill, *Introduction to Quantum Computation and Information*, H.-K. Lo, S. Popescu, and T. Spiller, eds. (World Scientific, 2000).